System Design of a Quadrupedal Galloping Machine

J. Gordon Nichol
Surya P.N. Singh
Kenneth J. Waldron

Stanford University
424 Panama Mall, Bldg 560
Stanford, CA 94305, USA
jgnichol@stanford.edu

Luther R. Palmer III
David E. Orin

Ohio State University
Department of Electrical and Computer Engineering
2015 Neil Avenue
Columbus, OH 43210, USA

Abstract

In this paper we present the system design of a machine that we have constructed to study a quadrupedal gallop gait. The gallop gait is the preferred high-speed gait of most cursorial quadrupeds. To gallop, an animal must generate ballistic trajectories with characteristic strong impacts, coordinate leg movements with asymmetric footfall phasing, and effectively use compliant members, all the while maintaining dynamic stability. In this paper we seek to further understand the primary biological features necessary for galloping by building and testing a robotic quadruped similar in size to a large goat or antelope. These features include high-speed actuation, energy storage, on-line learning control, and high-performance attitude sensing. Because body dynamics are primarily influenced by the impulses delivered by the legs, the successful design and control of single leg energetics is a major focus of this work. The leg stores energy during flight by adding tension to a spring acting across an articulated knee. During stance, the spring energy is quickly released using a novel capstan design. As a precursor to quadruped control, two intelligent strategies have been developed for verification on a one-legged system. The Levenberg–Marquardt on-line learning method is applied to a simple heuristic controller and provides good control over height and forward velocity. Direct adaptive fuzzy control, which requires no system modeling but is more computationally expensive, exhibits better response. Using these techniques we have been successful in operating one leg at speeds necessary for a dynamic gallop of a machine of this scale. Another necessary component of quadruped locomotion is high-resolution and high-bandwidth attitude sensing. The large ground impact accelerations, which cause problems for any single traditional sensor, are overcome through the use of an inertial sensing approach using updates from optical sensors and vehicle kinematics.

KEY WORDS—gallop, intelligent control, quadruped, fuzzy logic

1. Introduction

Gallop gaits are biological adaptations employed by two classes of biological quadrupeds. These classes have been termed “cursorial” and “non-cursorial” (Jenkins 1971). They are distinguished by their musculoskeletal geometries and locomotive behaviors. Cursorial animals typically have a narrow stance relative to the height of their center of gravity. This narrow stance gives less inherent stability and more maneuverability. Most quadrupedal mammals having a mass above 5 kg (e.g., the horse (*Equus*) and dog (*Canus*)) are of this type. With few exceptions, e.g., the elephant (Hutchinson et al. 2003), etc., cursorial animals transition from walk to trot to gallop as speed increases (Heglund, Taylor, and McMahon 1974; Hoyt and Taylor 1981). Non-cursorial animals tend to have a wide stance relative to the height of their center of gravity. This sprawled stance gives more inherent stability. The tortoise (*Testudo*) and crocodile (*Crocodilus*) are of this type. Non-cursorial animals may not use gallop gaits at high speed (e.g., Renous et al. 2002).

Gallop gaits, whether used by cursorial or non-cursorial animals, have several features. First, gallop gaits are asymmetric (Hildebrand 1977). In a gallop, each of the legs is used individually, so that footfalls occur at significantly uneven time intervals within each stride. As a result, the gallop

The International Journal of Robotics Research
Vol. 23, No. 10–11, October–November 2004, pp. 1013-1027,
DOI: 10.1177/0278364904047391

does not have the paired foot symmetry that can be exploited to facilitate control (Raibert, Chepponis, and Brown 1986). Secondly, the gallop has one of two footfall patterns: rotary and transverse. In a rotary gallop, footfalls occur in a rotating sequence, with the first hind footfall occurring on the same side as the last fore footfall. In a transverse gallop, footfalls occur in an alternating sequence, with the first hind footfall occurring on the opposite side as the last fore footfall. For example, the sequence front-left, front-right, rear-left, rear-right is one of two possible transverse gallop gaits. The sequence front-right, front-left, rear-left, rear-right is one of two possible rotary gallop gaits.

The gallop gaits, when used by cursorial animals, have two additional features. First, they are used at high speed (Alexander and Jayes 1983; Heglund and Taylor 1988) to minimize energy expenditure (Hoyt and Taylor 1981) perhaps because, like the trot, gallop gaits exhibit relatively small pitch excursions compared to the bound (Raibert 1990). Secondly, cursorial gallop gaits of either kind increase stride length, and thus speed, by using at least one and often two flight phases per stride (Gambaryan 1974).

A quadrupedal machine capable of a cursorial gallop would be able to travel with relative efficiency at high speed on smooth level ground, and potentially negotiate rubble piles, jump obstacles, etc. In a cooperative effort to better understand the cursorial quadruped gallop gaits, Ohio State University (OSU) and Stanford University have constructed an artificial quadruped. Construction of the quadruped has been preceded by several single-leg and full-quadruped simulations (Marhefka and Orin 2000; Marhefka et al. 2003), and three single-leg mechanical prototypes. It is planned that this quadruped will produce a fully cursorial gallop. Poulakakis, Smith, and Buehler (2003) have reported on the execution of a rotary footfall sequence by their artificial quadruped, but the gait appears to lack the other features of a cursorial gallop.

The Stanford group, under the direction of Dr Kenneth Waldron, has responsibility for designing a suitable sensor system and continuing the mechanical design work begun at OSU. The OSU group, under Dr David Orin, is working to develop a control system for this quadruped.

In the next section we describe the mechanical design of the system. In Section 3 we present the control system implemented and in Section 4 we discuss the sensor system. The paper concludes with a discussion, in Section 5, of some of the results.

2. Mechanical Design

The quadruped body and legs must be designed to meet several criteria. A first reaction to designing such a quadruped would lead the designer to mimic, as closely as possible, a biological quadruped. Although extensive data on biological quadrupeds are available (Gambaryan 1974; Pandy et al. 1988), a purely biomimetic approach would impose such stringent requirements on actuator and structure as to be impracticable. Instead, we have attempted to identify characteristics of biological quadrupeds essential to the gallop.

Some of the important characteristics we have identified are as follows. It is important for a galloping machine leg to store kinetic energy as it is compressed and to release that energy as it extends (Alexander 1988). A leg should have a means of adding a controllable amount of energy at each ground contact to compensate for impact and other losses. Energy storage and addition should be independent of each other and independent of leg length. Additionally, legs should exhibit a nonlinear stiffness to minimize leg excursion (Schmiedeler and Waldron 2002), and have a mass distribution and geometry which minimize impact loss (Schmiedeler and Waldron 2000). A cursorial gallop requires that a machine have cursorial geometry. The mechanical design of the quadruped described below has many of these features.

2.1. Quadruped

Although a biomimetic quadruped may include design elements characteristic of both cursorial and non-cursorial animals, a true hybrid design may not benefit from the advantages of either class. Overall geometry is an early design consideration.

Another early consideration is scale (Alexander 1985). Suppose a machine increases in size with respect to some linear dimension. As this linear dimension increases, area, which is related to actuator authority for most actuation technologies, increases as the square of the linear dimension. Similarly, volume, which affects mass and inertia, increases as the cube of the linear dimension. In other words, as size increases, actuator authority decreases relative to mass. On the other hand, reducing size tends to result in poor power system efficiency, and runs against the lower limits of available component sizes. Additionally, reducing size increases characteristic frequencies, which may necessitate a disproportionate increase in actuator power.

The quadruped is called the KOLT (kinetically ordered locomotion test) vehicle. The term "kinetically ordered" refers to the determination of the order and phase of the leg movements by the kinetics of the vehicle body (Schmiedeler and Waldron 1999). A complete discussion of the KOLT vehicle design decisions is beyond the scope of this paper. Tradeoffs lead us to design a cursorial quadruped which is roughly the size of a large goat (*Capra*) or antelope (*Antilope*). Actuation is electromagnetic. The total mass budget for the quadruped is 75 kg. At rest, the leg length from foot to hip is 0.68 m.

The quadruped is shown in Figure 1. Each three-degree-of-freedom leg is a module. The modules can be connected in a variety of configurations. This modularity will allow for future tests of leg location, leg orientation, and body flexion. The top surface of each module serves as a mounting platform

Fig. 1. KOLT vehicle.

Fig. 2. The OSU DASH leg, attached to test boom.

for motor amplifiers, power supplies, and control computers. This platform permits easy assembly, diagnosis, repair and reconfiguration of the electrical subsystem.

2.2. Construction Methods

A galloping machine must be able to withstand the foot–ground impact loads imposed by galloping. It must also be robust to dynamic mishaps. The selection of materials and construction methods becomes a very important early step. After considering many options, we chose methods and materials employed by the light aircraft industry in constructing stressed-skin aluminum airframes. Using these methods (Bingelis 1986; Department of Defense 2004; Federal Aviation Administration 2004), sheet aluminum can be cut, bent, and riveted into structures.

These methods were chosen for several reasons. First, they are capable of creating structures of high stiffness and strength relative to weight. Because these structures are fabricated from cold-rolled or strain-hardened sheet aluminum, they have a higher stiffness than a machined part of the same geometry. Additionally, thin sections can be easily fabricated. These thin sections can be located far from a neutral axis to provide high strength for a given amount of material.

Secondly, structures correctly designed with these methods are highly vibration resistant. Riveted joints are assembled by plastically deforming the fasteners. This plastic deformation applies a pre-load to the parts being joined. A correctly designed riveted joint will not loosen under vibration. Additionally, rivets are often made of aluminum; threaded fasteners are usually made of steel. Rivets provide a weight savings when used as a substitute.

Thirdly, parts which have been punched or laser-cut and subsequently folded on equipment can be assembled with little loss in accuracy. Assembly is relatively simple, requiring only the tools necessary for riveting. Correctly designed parts are self-fixturing.

Fourthly, these methods are adapted to produce small quantities of parts economically. Materials and fabrication are relatively inexpensive. Assembly is rapid and requires no tooling. Rivet removal is nearly as fast as removing a threaded fastener.

2.3. Single Leg

Once overall size was established, the quadruped was designed literally from the ground up. Schmiedeler designed the OSU DASH (dynamic articulated structure for high performance) leg (Schmiedeler 2001; Schmiedeler and Waldron 2002), based on work carried out by Brown and Zeglin (1998) and others (Mennitto and Buehler 1996; DeMan, Lefeber, and Vermeulen 1998; Kimura, Akiyama, and Sakurama 1999). The Stanford DASH leg, the second prototype, was developed at Stanford University (Figure 3; Nichol and Waldron 2002). The final leg, a slightly modified version of the Stanford DASH leg, also developed at Stanford University, can be seen installed in the body in Figure 1.

One divergence from biomimesis is the choice, made early in the project, to design only one leg to serve as both fore and hind leg. In natural quadrupeds, the roles of the fore and hind legs are quite different (Pandy et al. 1988). In spite of this difference, a single leg has been designed which will fill both roles. Using a single leg reduces the number of different

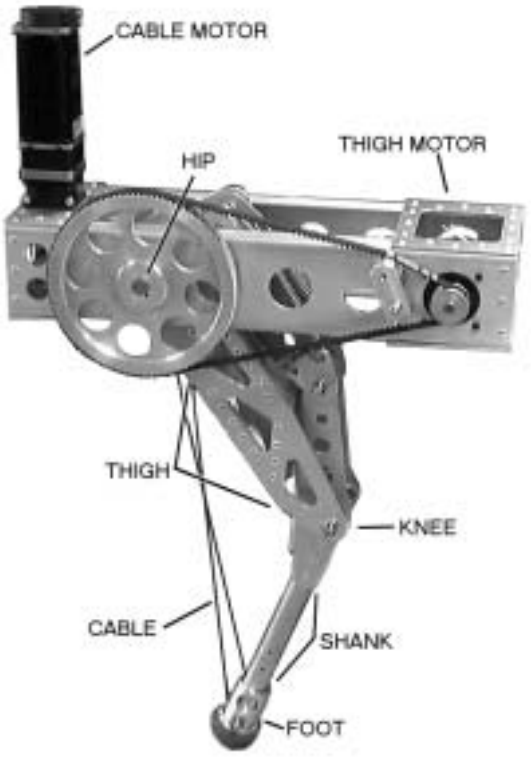

Fig. 3. The Stanford DASH leg with nomenclature.

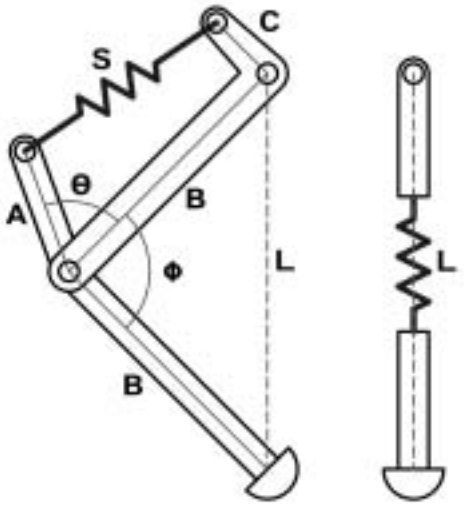

Fig. 4. DASH leg (left) and comparable virtual leg (right).

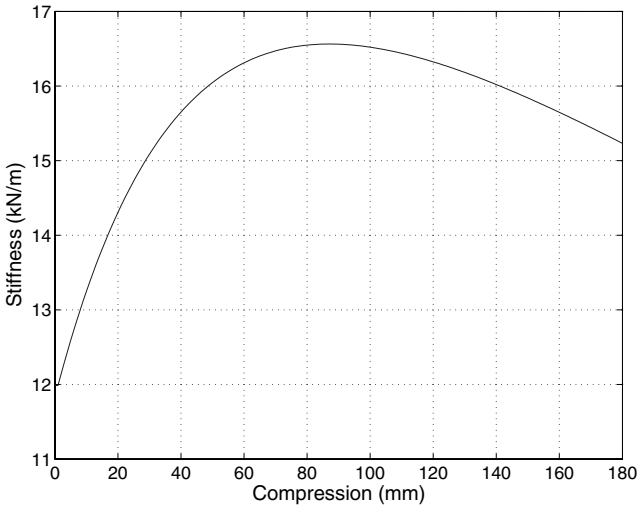

Fig. 5. Virtual leg compression versus stiffness (Schmiedeler 2001).

parts in the final machine, and reduces single-leg testing by one-half.

The names chosen to identify parts of the single leg (Figure 3) were drawn from animal anatomy and represent a mix of fore and hind leg nomenclature. This mix is appropriate, as the same leg serves for both.

With each leg prototype, features were incorporated and refined. Three of the most important design features found in the Stanford DASH leg are nonlinear effective stiffness, the over–under cable linkage, and the quick-release capstan.

2.3.1. Nonlinear Stiffness

The functional leg geometry has nonlinear virtual stiffness. The leg mechanism (Figure 4, left) can be modeled as a prismatic leg (Figure 4, right) with nonlinear stiffness (Figure 5). As the leg is compressed, the leg stiffness initially increases sharply until approximately 47 mm (15.9 kN m^{-1}), and then remains roughly constant. This variable stiffness allows us to keep the leg operating length relatively short.

2.3.2. Over–Under Cable Linkage

In order to avoid coupling the thigh and cable axes, a cable linkage was developed which separates the two axes by applying equal and opposite moments about the hip (Figure 6).

One end of the cable is attached to a fixed anchor. The cable passes under, then around the first of two pulleys at the hip. The cable is then looped around the ankle pulley, and over the second hip pulley. Finally the cable is attached to the capstan.

This cable drive gives a 2:1 force reduction with relatively little loss. Cable tension is half as large as the virtual spring force.

We are currently using ultra-high-molecular-weight polyethylene (UHMWPE) (Spectra®2000) cable. This cable is constructed with a unidirectional UHMWPE core covered

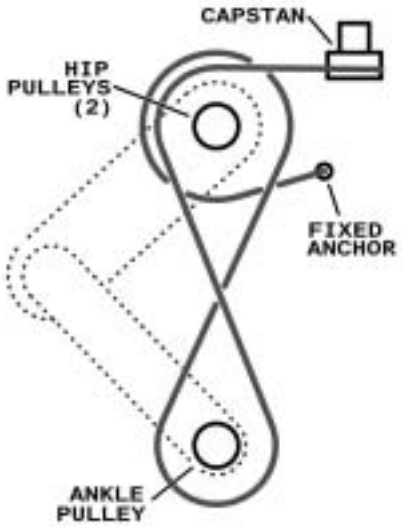

Fig. 6. Cable linkage.

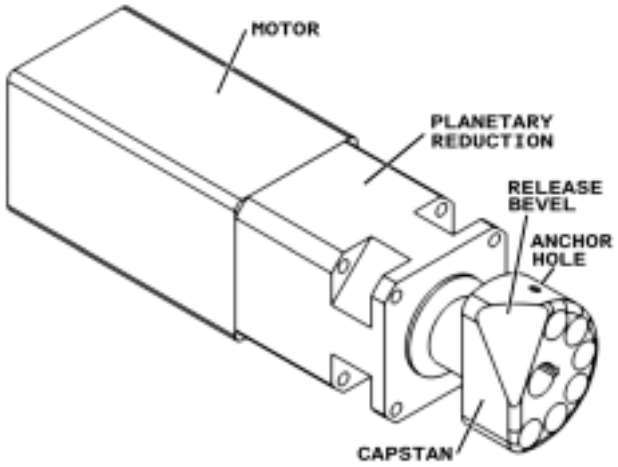

Fig. 7. Cable actuator with capstan.

by a tightly braided jacket of the same material. The line is of the type used with kite boards. It has a very high stiffness of 113 GPa, an ultimate tensile strength of 2.7 kN (Honeywell International, Inc. 2002) and a diameter of 1.8 mm. Additionally, UHMWPE does not self-abrade, making it an excellent choice for this cable drive.

After much difficulty, it was found that the "Anglers Loop" and the "Figure-Eight," backed by an overhand knot do not slip or weaken significantly with use. See Ashley (1953) knot numbers 1017, 520, and 514, respectively. The ends of the cable were heated to fuse the fibers before tying the knots.

2.3.3. Cable Drive Capstan

Initial attempts to employ an electromagnetic clutch to release the cable have shown that the majority of clutches cause large energy losses and are excessively slow. Electromagnetic brakes suffer from similar disadvantages. One successful strategy was to hold the cable motor in a stall after cable windup, and then to reverse the motor as ground contact was detected. This method was effective; however, the tradeoff between winding torque, reversal speed, and stall current leads to a very inefficient actuator. The quick-release capstan drive was designed to overcome this problem.

The cable drive capstan attaches to the end of the cable actuator (Figure 7). The hole through the center of the capstan, with the rectangular groove (keyway), fits over the output shaft of the planetary reduction. The holes surrounding and parallel to the grooved hole reduce cam weight and allow access to the back of the anchor hole. The cylindrical surface, small-radius surface, flat surface, and oblique flat surface (release bevel) on the outside of the cam are the four functional surfaces.

In operation, the capstan rotates counterclockwise as seen in the figure, so that the cable winds behind the capstan. At rest, the cable extends radially from the anchor hole. As the capstan begins to rotate, the cable is drawn from the leg, causing the leg to shorten, and the springs to store energy. After the first 90° of capstan rotation, the cable is tangent to the cylindrical surface of the cam. After another 180° of rotation, the cable has wrapped completely around the large cylindrical surface and begins to wrap around the small-radius surface which joins the cylindrical face with the flat face. Another 70° brings the cable parallel to the flat face of the capstan. In this position, the cable is relatively close to the center of rotation of the capstan, decreasing holding torque. When the foot contacts the ground, the capstan rotates an additional 20°–40°, forcing the cable down the release bevel and off the cam.

The capstan adds one full twist to the cable at each release. This twist, if left unchecked, would result in premature cable failure. A swivel was added between the hip and ankle pulleys to prevent twist accumulation.

It is desirable to find a capstan geometry which, at the same time, minimizes the actuator torque required to hold the cable under tension, and allows control over the amount of cable wrapped around the capstan each time. For this type of capstan, holding torque and cable wrap variability requirements are in opposition. A small holding radius (holding radius being the length of the common normal between the cable centerline and the capstan rotational axis) requires a small torque to hold a given cable tension. A small holding radius makes the cable length relatively insensitive to capstan rotation. A large holding radius requires a larger torque to hold the same cable tension. A large holding radius makes the cable length more sensitive to capstan rotation. The power required to maintain holding torque is wasted, as it does nothing to add energy to each stride. The capstan is currently designed to favor efficiency.

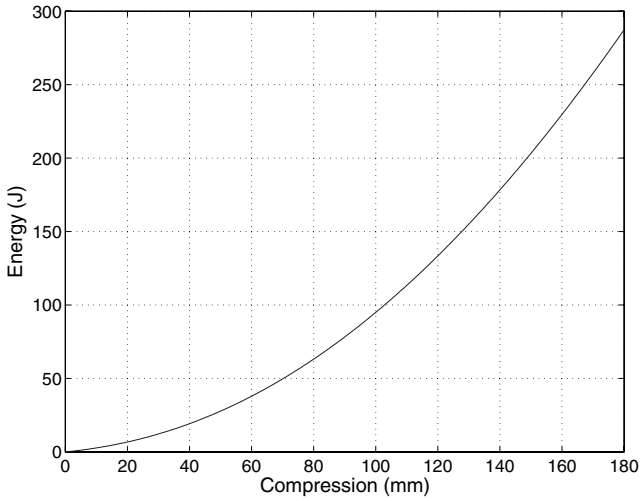

Fig. 8. Leg spring energy storage as a function of leg compression.

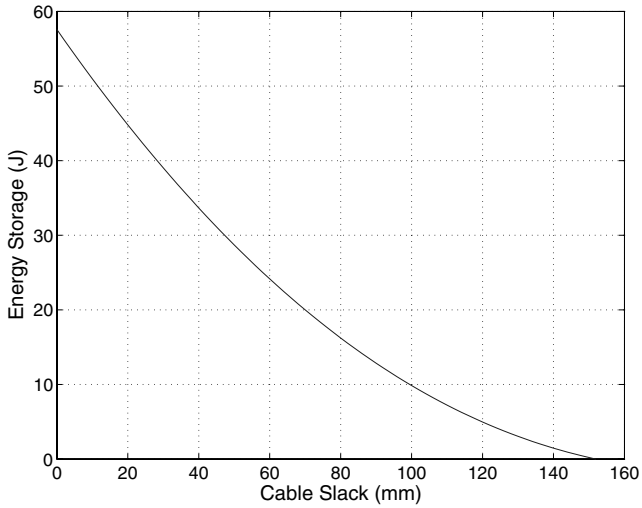

Fig. 9. Cable slack length and its effect on the per-stride energy addition.

The cable actuator was chosen so that it can rotate only as far as necessary to release the cable during the short (50–80 ms) ground contact. This means, as stated above, that the cable actuator cannot take in significantly less than the capstan design cable length of 15 cm. This constant cable length makes leg length at each ground contact a constant, which eases control system design. Strategies to control energy addition are being investigated.

Figure 8 shows the amount of energy which can be stored in the leg as a function of length L. Maximum energy storage (290 J) is set by strain limits on the coil springs being used.

Because the capstan takes in the same amount of cable each cycle, the slack cable length has a large effect on total energy addition. Figure 9 shows that, as the length of slack cable increases, the energy which can be stored in the springs decreases. The total energy which can be stored in the springs is most sensitive to changes in cable length when the cable has zero slack (see Figure 17). One strategy for controlling energy addition is to control cable slack.

2.4. Results

Single-leg testing was accomplished differently at Stanford and OSU. The Stanford DASH leg and its successor were tested as they ran in a circle. The OSU DASH leg was tested on a treadmill. Both legs were constrained by test booms to be quasi-planar. All leg tests were accomplished by running the leg knee-backward, measuring forward velocity to the left in Figure 3. The quadruped may also use the knee-forward configuration, but the results of only one knee direction are presented here.

The current top speed of a single leg is 4.15 m s^{-1}. Different gaits are more efficient at different speeds. According to Hoyt and Taylor (1981), horses transition between trot and gallop at about 4.5 m s^{-1}. Using the dynamic similarity hypothesis of Alexander and Jayes (1983), and an estimate (Hoyt and Taylor include mass ranges for their test subjects, but no measurements) of the relative size of the horse and the KOLT vehicle, 4.15 m s^{-1} is slightly above the KOLT vehicle trot–gallop transition speed. Another result, from Heglund and Taylor (1988) predicts a trot–gallop transition speed of 3.9 m s^{-1}. The current single-leg top speed of 4.15 m s^{-1} will allow the quadruped to gallop efficiently.

3. Control System

Raibert (1986) has shown that the airborne trajectory of a single-leg machine is determined by the horizontal placement of the foot relative to the hip and the energy in the springs at touchdown. The thigh angle and length of cable drawn in before ground contact dictate these two parameters on the Stanford DASH leg, so cable draw and hip angle are the two outputs of each controller developed. Achieving good performance here is more difficult, though, because of the articulated leg structure as opposed to the prismatic structure used by Raibert.

However, Raibert's controller must be modified to function satisfactorily in a quadrupedal gallop. The concept of putting energy into the system by means of the vertical thrust component results in significant variations in the stride period. In order to execute a stable gallop it is important that the stride period at any given speed be approximately constant. This implies that the total vertical impulse from the leg contacts is constant, since the period of a ballistic trajectory is determined by the initial vertical velocity component. The

total vertical impulse is the product of the stride period and the weight of the machine, and is therefore constant for constant stride period. Hence, the controller must work with the horizontal impulse component.

The leg cycle begins when the controller is called at the top of flight (TOF), the highest vertical point in the leg's ballistic flight trajectory. The controller computes new outputs based upon present and desired body states, and experimentally tuned PID controllers drive the joints of the leg to the desired positions. The joint controllers continue actuation until the foot detects ground contact. At this point, the actuator at the hip is turned off to allow the thigh to undergo its natural response and the cable motor is driven forward to a position allowing the cable to slip off of the specially designed capstan. When the foot no longer detects ground contact, the joint actuators use the previous TOF outputs as setpoints and wait for new inputs after the next top of flight.

3.1. Control System Design

Legged machines are quickly growing in complexity to accomplish more demanding tasks, such as, in this case, galloping at high speeds. Accurately modeling these complex machines operating with asymmetric footfalls in dynamic trajectories becomes difficult, and control techniques based on the system model can yield poor results. Intelligent controllers do not require system identification and can incorporate user heuristics to successfully control this type of system. Intelligent controllers can require more computational power, which has previously limited their use in real time. In this work, two intelligent methods are implemented in real time on the Stanford DASH leg and compared with each other and against a more traditional control algorithm. The first controller tested is a heuristic algorithm whose parameters are updated in real time by the Levenberg–Marquardt (LM) learning method, and the second is a direct adaptive fuzzy controller.

3.1.1. Heuristic Control with Levenberg–Marquardt Learning

Raibert's original controller computed the forward touchdown position of the foot by

$$x_f = \frac{vT_s}{2} + k_v\,(v - v_d)\ , \tag{1}$$

where T_s is the time of the previous stance period, v is the TOF body velocity, and v_d is the desired TOF velocity. The gain on velocity error, k_v, is tuned experimentally for desired performance. The first term of this equation estimates the foot placement required for running at constant speed and the second term corrects velocity errors. This equation is the result of some dynamic modeling performed by Raibert. By observation, stance time does not vary much so $T_s/2$ can be included in one coefficient for v.

The non-symmetrical leg requires an offset term added by Marhefka (2000) to maintain zero velocity. The new heuristic control equation, with a change in coefficient names, is

$$x_f = \alpha_1 v + \alpha_2\,(v - v_d) + \alpha_3\ . \tag{2}$$

The offset term α_3 is experimentally tuned. The LM on-line learning method is used to train the remaining two parameters, α_1 and α_2.

The error signal, ε, to be minimized is

$$\varepsilon = y - F\,(\boldsymbol{p}, \boldsymbol{\alpha})\ , \tag{3}$$

where y is the unknown best forward foot touchdown position for the present and desired system states, **p**. The function F(**p**, $\boldsymbol{\alpha}$) represents eq. (2) as the output of the heuristic controller dependent on α_1 and α_2. The LM algorithm is a derivative of the Gauss–Newton learning method used to solve least-squares problems (Jang and Mizutani 1996). The derivation of this algorithm for a one-leg machine is outlined in (Palmer et al. 2003). The resulting update formula for our system is then

$$\alpha_{j+1,m} = \alpha_{j,m} + \frac{p_m}{p_m^2 + \lambda_m} e_j \quad m = 1, 2 \tag{4}$$

where e_j is the system error, λ_m are step size control variables, $p_1 = v$, and $p_2 = (v - v_d)$.

λ_1 and λ_2 are components of the LM algorithm that do not exist in the Gauss–Newton method. These added parameters correct the ill-posed case of very small state parameters, **p**, and are also used to control the adaptation step size. The error, ε, in eq. (3) is not available for computing updates. Because of their monotonic relationship, the system error, $e = v_d - v$, is used instead of ε with good results. This is verified later in the results. The update is computed immediately before the controller is called at the beginning of the next cycle. The new coefficients, $\boldsymbol{\alpha}_{j+1}$, are then used in eq. (2) to compute the setpoints for the following touchdown.

3.1.2. Fuzzy Control with Direct Adaptive Learning

The fuzzy controller consists of a rule base, inference mechanism, fuzzification interface, and defuzzification interface. Figure 10 is a block diagram of the control process with an adaptation mechanism which will be described later. The fuzzy control process starts with fuzzification by mapping an input into one or more membership functions. Examples of triangular input membership functions used to characterize the desired change in body velocity, Δv_d, are shown in Figure 11. One membership function is centered at 0.0 m s^{-1} and will have a certainty, $\mu_{0.0}^{\Delta v_d}$, of 1.0 if the input lies at the center. If the desired change in body velocity is 0.125 m s^{-1}, then $\mu_{0.0}^{\Delta v_d} = \mu_{0.25}^{\Delta v_d} = 0.5$, and all other membership functions for that input become zero. The membership functions at both ends are saturated to include the entire range of input values. Using triangular membership functions without center overlap limits the number of non-zero membership certainties, for

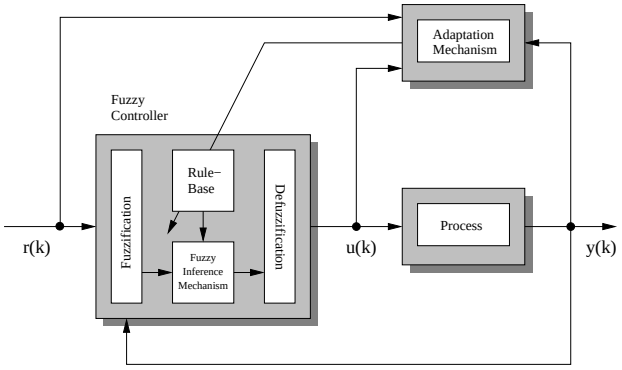

Fig. 10. Structure of the direct adaptive fuzzy control system (Marhefka and Orin 2000).

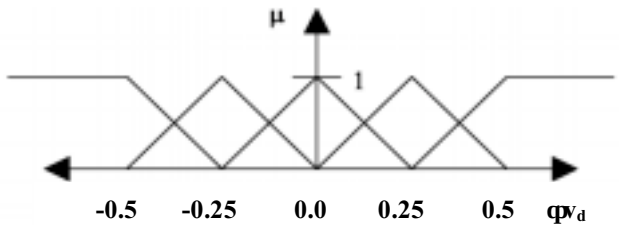

Fig. 11. Example membership functions for the change in desired leg velocity.

each input, to two. This reduces the computational complexity of the fuzzy controller.

The actual membership function centers used in the control system are shown in Table 1. The body velocity, v, the desired change in velocity, Δv_d, and height, h, make up the three inputs to the controller.

The fuzzy rule base is a table of controller outputs for every combination of input membership functions. The number of rules is then equal to the product of the number of membership functions for each input. For our controller there are $7 \times 5 \times 5 = 175$ rules, each with a corresponding output for touchdown thigh angle. For the results given in the paper, the cable length was not varied so energy added to the system each cycle remained constant.

The inference mechanism is the next step in the fuzzy controller. This mechanism determines the applicability of each rule to the current inputs. The product is used to determine the certainty, μ_i, that the premise of rule i is currently applicable. The certainty of rule i whose premise is

if velocity is "0.0 m s^{-1}" and desired change in

velocity is "0.25 m s^{-1}" and height is "75 cm"

would be

Table 1. Fuzzy Controller Input Membership Functions

Input	Membership Function Centers	Units
v	–1, 0, 1, 2, 3, 4, 5	m s^{-1}
Δv_d	–0.5, –0.25, 0, 0.25, 0.5	m s^{-1}
h	70, 75, 80, 85, 90	cm

$$\mu_i = \mu_{0.0}^{v} \times \mu_{0.25}^{\Delta v_d} \times \mu_{75}^{h}. \quad (5)$$

As mentioned earlier, each input has a maximum of two non-zero membership certainties so the number of rules with non-zero premise certainties becomes 2^n, where n is the number of inputs. Adding membership functions to an input will not affect the amount of computation because only two membership functions are on, in each input. Adding inputs, however, will significantly increase computation.

The last element of fuzzy control is defuzzification. This process combines the recommendations of each rule in an output based upon rule certainties. Center average defuzzification is used and the output y is given by

$$y = \frac{\sum_i c_i \mu_i}{\sum_i \mu_i}, \quad (6)$$

where μ_i is the premise certainty of rule i, and c_i is the output of rule i. This equation shows a summation over all rules. Each rule output center is multiplied by its certainty, which weights the controller output toward the rule most applicable. This controller uses three inputs, meaning that only the eight rules with non-zero premise certainties need to be included in eq. (6).

3.1.3. Adaptation Mechanism

The adaptation mechanism modifies the rule output centers to correct velocity errors. Immediately before the controller is called, the current system state is compared to the desired state calculated at the previous TOF. The output for rule i, c_i, is updated as a factor of this error by

$$c_{i,j+1} = c_{i,j} + K_c \mu_{i,j} e_j, \quad (7)$$

where K_c is the adaptation gain, $\mu_{i,j}$ is the certainty of rule i at the jth cycle, and $e_j = v_d - v$ is the system error of cycle j. K_c is tuned experimentally. Note that the certainty of rule i is used to scale its update. This applies more change to the rule outputs that were more applicable. Again, this premise certainty is non-zero for only 2^n rules, meaning that only the rules that applied to the previous controller output are updated by the

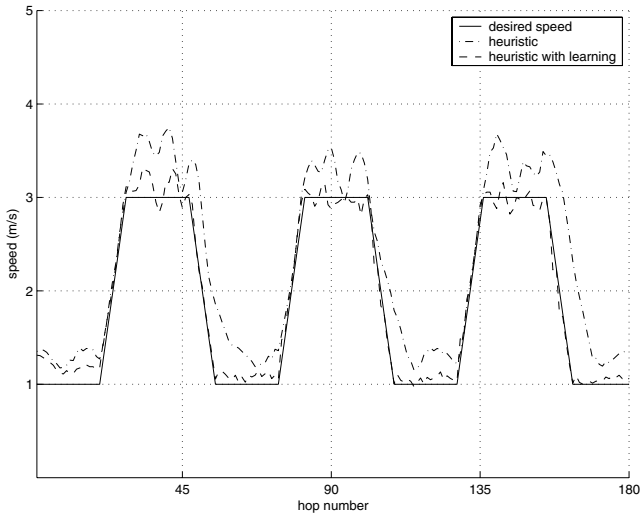

Fig. 12. Heuristic control compared with learning on and off.

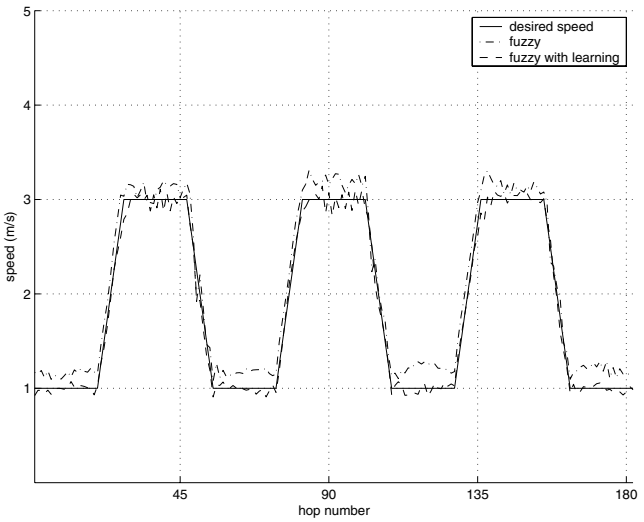

Fig. 13. Fuzzy control compared with learning.

present error. In this adaptation mechanism, the foot is placed further forward if the velocity is too high. This method is a direct result of the user's heuristic knowledge of the system.

The direct adaptive approach is computationally simple enough to run in real time. This method also utilizes heuristics to eliminate the need for difficult system identification and added complexity in the algorithm equations. The controller can also adapt to changes in leg configuration without the need for major restructuring.

3.1.4. Results

The real-time control is implemented on a Kameleon board from K-Team, which has a Motorola MC68376 microcontroller running at 20 MHz and without hardware support of floating point operations. Body velocity is measured by applying a simple Butterworth filter to the Euler derivative of incremental encoder counts on the boom vertical axis.

Figure 12 shows the leg response to heuristic control without learning compared to the response of heuristic control with on-line LM learning. The initial values for α_1 and α_2 were hand tuned for reasonable performance. Without LM learning, the leg slowly responds to changes in the desired velocity, and steady-state error is observed. The large velocity errors exhibited with learning turned off are quite similar in size to those reported by Raibert (1990). With learning on, the steady-state error is decreased and a faster response to desired velocity changes is noticed.

Figure 13 shows the response of the leg using a fuzzy controller with and without direct adaptive learning. The rules shown in Table 1 were used in both cases shown. The fuzzy controller with learning outperforms the fuzzy controller without learning and the heuristic controller with learning. This is expected because the fuzzy controller stores more parameters. The precision control of the fuzzy algorithm is a tradeoff to the computational simplicity and small memory footprint of the heuristic controller.

As described earlier, eight rules have non-zero premise certainties in the case of three inputs. The non-zero certainties are used to calculate a fuzzy output and also update individual rule outputs. In order to test the performance of the leg when the number of inputs and rules are reduced, the height input in Table 1 was eliminated. The new controller has $7 \times 5 = 35$ rules which occupy less space in memory, and only four rules have non-zero premise certainties for a given set of inputs. The response of the leg using the simplified fuzzy controller is shown in Figure 14 with the response using the extended-rule set. With fewer rules, the performance is degraded but may still be acceptable. Although not shown, the body height varied more during tests when height was not used as an input to control the system. The performance of the reduced-rule fuzzy controller closely matches that of the heuristic controller with LM learning, although it is expected to do better. During these tests of mainly two speeds, only a limited number of fuzzy rules are activated. The fuzzy controller is expected to show superior performance during a more extensive test covering more speeds, which also degrades the performance of the heuristic controller.

The LM algorithm significantly improved the performance of the heuristic controller. The update laws for the LM algorithm were derived from the heuristic control equation, which is based on Raibert's original equation for the forward touchdown position of the foot. Although simplified, the heuristic algorithm was based on the actual dynamics of a one-leg system. At the time of writing, there was no corresponding set of equations modeling a three-dimensional quadruped. It is

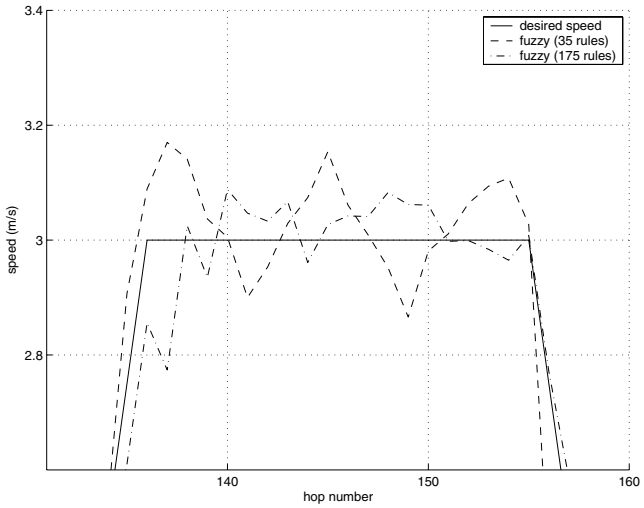

Fig. 14. Original fuzzy controller compared with a smaller rule base controller.

planned to produce an adequate controller without needing these equations, allowing the intelligent controller to create its own mapping.

The fuzzy controller outperformed the heuristic controller without relying on a model of the system. The direct adaptive fuzzy controller uses heuristic update laws to create its own mapping of input leg configuration to output body state. A reduced-rule base fuzzy controller also performed well on the Stanford DASH leg.

The fuzzy controller can be extended for use on the quadruped by applying similar heuristics. Marhefka simulated a planar quadruped with prismatic legs galloping close to 7 m s^{-1} using the direct adaptive fuzzy approach (Marhefka et al. 2003). Intelligent controllers and learning algorithms will continue to prove themselves a valuable asset towards the development of a galloping quadruped.

4. Sensors

To propel itself and execute the maneuvers necessary for galloping, the KOLT vehicle must accurately and rapidly perform a complex series of motions. In order to maintain controllability and quantify the galloping motion, the on-board sensing needs to robustly capture the internal state, foot–ground contact, and vehicle position and attitude with respect to the ground.

Although similar to sensing problems in dynamic vehicles (e.g., autonomous helicopters and unmanned ground vehicles), sensing in the KOLT vehicle is unique due to the scale and nature of dynamic legged locomotion (Waldron et al. 2003). The locomotion domain is characterized by rapid state changes, large ground impacts, asymmetric impulses, and rapid force cycling. This challenges sensor design as these factors result in large dynamic range (i.e., high sensitivity over a large operating range) and low-latency requirements. However, this domain does allow for several novel corrective techniques including visual odometry/heading, cues from ground contact forces, and proprioception via leg kinematics.

4.1.1. Foot Contact Sensing

It is of principal importance to know when the foot has contacted the ground so as to initiate the next cycle by releasing the cable and to potentially update the position estimate relative to the ground. This is achieved by placing a force-sensing resistor (FSR) (Interlink Electronics) between the shank and the upper section of the foot assembly (see also Figure 15). This, in turn, causes the FSR to be compressed changing its resistance significantly. This change is detected by a comparator circuit, which sends the final digital signal to the controller. To distribute forces evenly over the active surface of the FSR, a rubber pad is placed over the sensor.

4.1.2. Position Sensing

The traditional approach to measuring position and attitude is via an inertial navigation system (INS). An INS operates on the principle of dead reckoning and is typically implemented using a triaxial accelerometer and a gyro triad. The major drawback of INS systems is the unbounded position estimate error due to integration errors and sensor noise (Necsulecsu et al. 1993).

Barshan and Durrant-Whyte (1995) have shown the applicability of an INS for mobile robots given the widespread availability of compact solid-state inertial sensors. Further, Kalman filters and other related algorithms allow for limited robotic operations without updates from an absolute source (Bachmann, Yun, and McGhee 2003). This is of importance as common navigation aids (e.g., GPS or magnetometers) do not provide sufficient spatial resolution, guaranteed availability (especially indoors), or the update rates needed to fully control the KOLT vehicle.

Robust motion sensing and position tracking with respect to the ground are needed for the control and further refinement of the KOLT vehicle. As discussed in Sections 2 and 3, the criteria for this sensor are stringent as the sensor system must operate such that it provides:

- robustness to large cyclic shock and vibration loads (withstand >20 g power-on shock), while maintaining linear acceleration measurements of ± 10 g on all axes;
- high-resolution attitude estimation ($< 0.5^\circ$ resolution and $> 360^\circ\ s^{-1}$ rates);
- fast update of final position/velocity estimates (>30 Hz);

- computational efficiency (for operation using embedded microprocessors).

Further design objectives include self-contained operation, a low noise floor, low mass (i.e., <0.1 kg), low power consumption (<5 W), and low cost (<$1500).

At first glance, an INS appears to be the ideal, if not the only, sensing methodology for this vehicle (Barshan and Durrant-Whyte 1995). The rigid mechanical design of the KOLT vehicle improves INS applicability by simplifying the calculations and allowing measurements about any single point to be extrapolated for the body. This provides flexibility in sensor placement as components need not be collocated. Further, recent developments in inertial micromachined sensors result in miniature inertial transducers that, although noisy, provide acceptable sensitivities such that an INS can be constructed at significantly reduced size and cost compared to traditional versions (Belloy, Sayah, and Gijs 2002).

An extensive survey of the literature and the commercial market for these sensors did not show an equally robust technological alternative. INS packages employing micromachined sensors are available from a variety of commercial vendors. In general, these units are designed for less demanding applications and need to be modified for the severe dynamic loads present during full-speed galloping. These units typically combine commercial sensing elements (i.e., accelerometers, gyros, and magnetometers) with proprietary integration and filtering software to yield a final sensed value that is communicated to a PC. This process adds delay and complicates the integration of these devices (Bachmann, Yun, and McGhee 2003). Thus, in areas with rapid dynamics, such as the legs, inertial sensors are directly used to obtain differential motions over very short time-steps.

4.1.3. Sensor System Design

The KOLT vehicle is equipped with both basic and integrated sensors in a layered architecture that provides quick initial responses followed by corrected estimates that factor in updates from (often slower) redundant measurements. The sensor architecture can also take advantage of the unique kinematic relations between the vehicle and ground frames present during ground contact in legged locomotion.

As shown in Table 2, numerous sensors are used on the KOLT vehicle at various levels of its operation. Internal state (i.e., joint position) is measured using precision 1000-count encoders on each motor. Attitude and position sensing relative to the ground is performed on the KOLT vehicle using a modified commercial INS whose values are quickened using a micromachined gyro and whose drift is checked via rough optical range measurements. On the Stanford DASH leg, this is performed using both an inertial technique based on inputs from a high-shock-rated thermal-based accelerometer that are checked using optical range measurements and, when available, through precision encoders on an experimental boom arm. Inertial techniques, while not as precise as fixed measurements, allow for self-contained operation of both the KOLT vehicle and the Stanford DASH leg and provide robustness by making operation independent of external measurements.

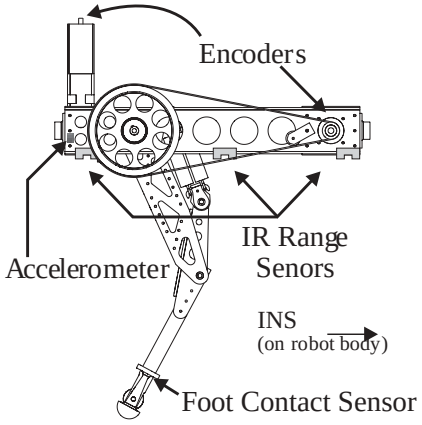

Fig. 15. Stanford DASH leg instrumentation.

4.1.4. Calibration and Drift Cancellation

Calibration of the inertial components is especially important as the micromachined sensors that make up the INS have significant temperature sensitivity and part-to-part variance. While these sensors have been thoroughly calibrated off-board, it is risky to solely rely on these calibrations while they are mounted on the vehicle, due to unknown variations such as those in temperature and supply voltage. Approximate on-board calibration can be performed at rest by measuring the gravitational acceleration. However, this assumes the output is a linear function of the acceleration and that the accelerometer's axes are properly aligned.

Since inertial navigation is fundamentally based on dead reckoning, it is highly susceptible to quadratically increasing drift from double integrating sensor, calibration, and alignment errors. For extended operations, it is practically necessary to correct this through updates from an absolute source. For the KOLT vehicle, traditional update sources are not applicable: GPS is not available for indoor operations; magnetometers are affected by the large, non-deterministic magnetic fields from the vehicle's actuators; and tilt sensors are gravity referenced and cannot distinguish between gravitational and inertial effects, especially in a dynamic environment such as the one encountered by this vehicle.

The KOLT vehicle sensor system addresses drift and sensor nonlinearity by comparing the estimate with those provided by the infrared range estimates of the distance of the vehicle to the ground. The use of these sensors for updates is complicated due to the sensor's nonlinear operation, noise, low-frequency operation (20 Hz), and numerous variances such as floor color

Table 2. Sensors on the KOLT Vehicle

Sensor	Measurement	Notes
Accu-Coder Model 755 (size 15)	Joint actuator (and boom arm) angles	Precision encoder: absolute joint positions are extrapolated from the actuator–joint couplings.
MEMSIC MXA2050AL	Acceleration	Dual-axis, thermal ±10g accelerometer: offers exceptionally high shock survival (50,000 g).
Silicon Sensing CRS03-11	Angular rate	Single-axis, up to 573° s^{-1}
Microstrain 3DM-G-ADI	Orientation estimation	INS: combines magnetometers, accelerometers, and angular rate sensors to give orientation data in the Earth (azimuth-elevation-roll) frame.
Sharp GP2Y0A02YK	Height (position)	Long distance, optical infrared range sensor. Slow and nonlinear. Used as update source to correct inertial estimates.

and surface texture. Sensor noise was moderated via a 20 Hz low-pass filter. By measuring the heights at two or more points on the same rigid frame, the position can be measured more robustly and an attitude update can be calculated based on geometric relationships between the points.

The inertial signals and updates were integrated using a Kalman filter mechanism that was slightly modified to handle the coupling between the distance measurement and variance for the infrared range updates. The Kalman filtering routines, which are initialized using sensitivities and sensor variances from the calibration routine, add delay to the estimates (Analytic Sciences Corporation 1974). When in contact with the ground, the KOLT vehicle can use proprioceptive measurements as a tertiary form of updates.

A best-available methodology is employed such that an estimate is presented and updated as further information becomes available. As shown in the composite flowchart in Figure 16, this can be performed via three distinct modes, as follows.

- **Short operation assumption mode.** This is the simplest and fasted method and estimates the position by simply integrating the inertial signals. While it has minimal delay, it is only helpful for relative changes.

- **Optical update and Kalman filter.** This method uses a filtered height update along with known statistics for the sensors to recursively estimate the vertical inertial sensitivity, offset, and additive noise (Analytic Sciences Corporation 1974). It assumes that the sensitivities are the same in both axes and this is used to correct the drift. The linear dynamic system used by the filter is shown in eqs. (8) and (9):

$$\begin{bmatrix} \dot{y} \\ \ddot{y} \\ \dot{r}_{bias} \end{bmatrix} = \begin{bmatrix} 0 & 1 & 0 \\ 0 & 0 & -1 \\ 0 & 0 & 0 \end{bmatrix} \begin{bmatrix} y \\ \dot{y} \\ r_{bias} \end{bmatrix} + \begin{bmatrix} 0 \\ 1 \\ 0 \end{bmatrix} a_{m_y} + w \tag{8}$$

$$y_m^{range} = \begin{bmatrix} 1 & 0 & 0 \end{bmatrix} \begin{bmatrix} y \\ \dot{y} \\ r_{bias} \end{bmatrix} + v. \tag{9}$$

  Here, y is the position estimate, $\dot{y}$ is the velocity estimate, $\ddot{y}$ is the acceleration estimate, r_{bias} is the offset, a_{m_y} is the measured acceleration, w is white noise, y_m^{range} is the infrared range update, and v is the noise model for the infrared range sensor.

- **Proprioceptive estimation/updates mode.** Because the vehicle makes cyclical contact with the ground, it is possible to use the kinematics of the leg joints as an additional update for error control. This quadrupedal proprioceptive (or "pedometric") filter operates by assuming the full kinematics of the vehicle are known. For the short amount of time during which the foot is in contact with the ground, the leg can be viewed as a kinematic chain between the ground and the vehicle center. This method is complicated, however, due to the compliance (albeit small) of the shank and foot placement uncertainty.

4.1.5. Experimental Validation

The KOLT vehicle sensor design combines multiple sensors to provide a fast estimate of the vehicle's state. In order to verify the operation of the self-contained design and in order to more fully characterize the vehicle's operation, a series of experimental operations were performed on the Stanford DASH leg using a laboratory boom arm. The six-foot long, stiff boom arm allows for two degrees of freedom (roll and

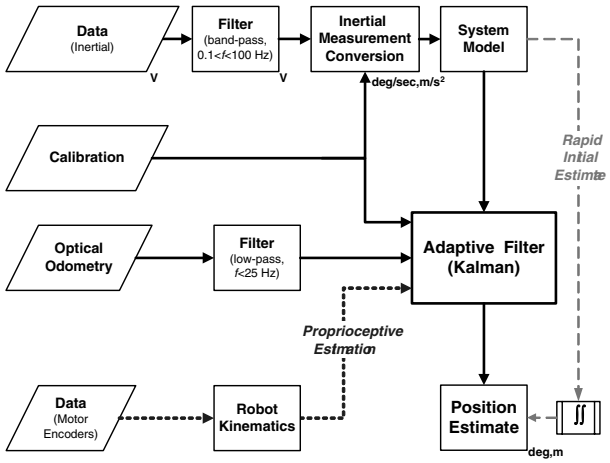

Fig. 16. Flow chart showing the data flow of the various estimation methods used by the KOLT vehicle and Stanford DASH leg. As updates come from the optical range sensors, the position estimate is updated. (The dashed line represents optional operations, units are shown in block subscripts.)

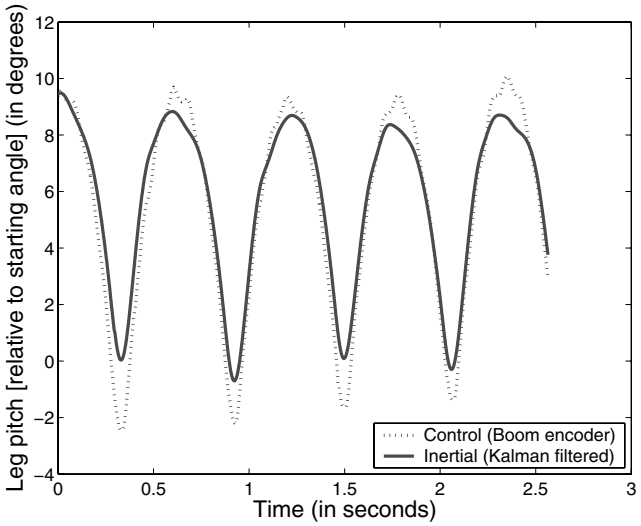

Fig. 17. Angular position estimation of single leg tests at 4 m s^{-1}. The error and delay of the Kalman-filtered inertial data (solid line) is evident as compared to control value calculated from boom encoders (dashed line). The root-mean-square error relative to the control for this selection is less than 1 degree.

yaw). It is instrumented using 6000-count precision encoders (see also Table 2) to give a spatial resolution of 5 mm.

The first set of experiments was used to calibrate and assess the quality of the sensor routines. For these experiments, data from the precision encoders are considered to be the control variable. In order to facilitate comparison, the Stanford DASH leg inertial estimates, calculated in the frame of the vehicle, were transformed to the boom arm origin. As shown in Figure 17, the sensing method tracked well except at the top and bottom of flight.

The second aspect of testing was to quantify the high-shock loads present during full speed robotic bounding with the Stanford DASH. Acceleration loads present depend on the energy stored in the springs, which is a function of the initial cable length. As shown in Figure 18, the impacts can be as high as 9 g (88 m s^{-2}). These data were used in the design of the KOLT to strengthen the shank and foot so as to support loads of nearly 10 times the body weight.

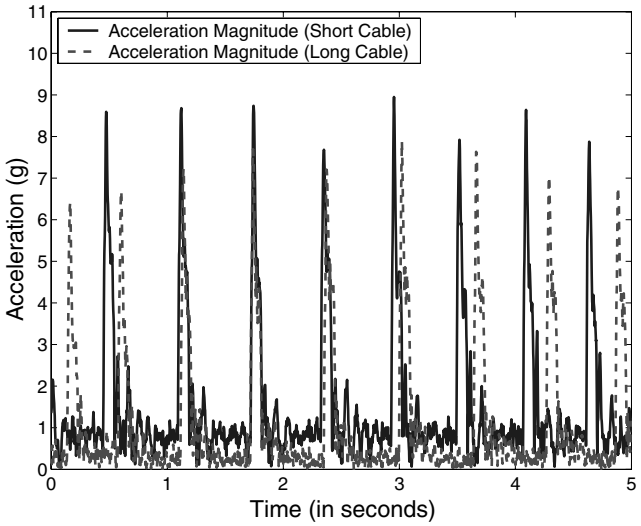

Fig. 18. Stanford DASH leg accelerations (in g) as a function of time (in s). As the cable is shortened, more energy is stored and the accelerations increase.

5. Discussion

The focus of this paper is the design of a leg for a quadrupedal galloping machine. At this point, the design of the leg is considered to be complete, including the design of suitable control algorithms, and the testing process is well advanced. The integration of four identical legs into the complete machine has been accomplished.

The use of electric actuation is attractive because of the simplicity of using batteries for a fully autonomous power supply for the complete machine, and the ease of control that is offered by electric actuation. However, the shortcomings of electric actuators for actively controlled oscillatory systems like this have also been very evident in this project. It is simply not possible to provide the intense power pulses needed from rotary electric motors without resorting to mechanical energy

storage that entails considerable complexity, and it is very challenging to design. It is noteworthy that Raibert's machines (Raibert 1986), which were of similar scale, used hydraulic, or hybrid actuation systems to bypass this issue. The problem then becomes one of living with a hydraulic hose tether, or providing an on-board hydraulic power supply, which poses challenges in dealing with weight, bulk and heat dissipation.

The dynamic environment of such a system also poses instrumentation challenges. These challenges range from simple ruggedness problems in an environment experiencing repetitive shock loading of the order of 10 g, to update rate, interfacing, and drift problems. Some of the solutions that have been tested on the leg require further development for the full three-dimensional requirements of the integrated quadruped.

Acknowledgments

The authors would like to acknowledge the support of the National Science Foundation Grant No. IIS-0208664, and of a National Defense Science and Engineering Graduate (NDSEG) program fellowship held by SPNS, in the conduct of this work.

References

Alexander, R.M. 1988. *Elastic Mechanisms in Animal Movement*, Cambridge University Press, Cambridge.

Analytic Sciences Corporation, Technical Staff. 1974. *Applied Optimal Estimation*, A. Gelb, editor, MIT Press, Cambridge, MA.

Alexander, R.M., and Jayes, A.S. 1983. A dynamic similarity hypothesis for the gaits of quadrupedal mammals. *Journal of Zoology, London* 201:135–152.

Alexander, R.M. 1985. Body support, scaling, and allometry. *Functional Vertebrate Morphology*, M. Hildebrand et al., editors, Belknap Press, Cambridge, pp. 26–37.

Ashley, C.W. 1953. *The Ashley Book of Knots*, Doubleday, New York.

Bachmann, E., Yun, X., and McGhee, R. 2003. Sourceless tracking of human posture using small inertial/magnetic sensors. *Proceedings of the IEEE International Symposium on Computational Intelligence in Robotics and Automation*, Kobe, Japan, pp. 822–829.

Barshan, B., and Durrant-Whyte, H.F. 1995. Inertial navigation systems for mobile robots. *IEEE Transactions on Robotics and Automation* 11(3):328–342.

Belloy, E., Sayah, A., and Gijs, M. 2002. Micromachining of glass inertial sensors. *Journal of Microelectromechanical Systems* 11(1): 85–90.

Bingelis, A. 1986. *Sportplane Construction Techniques*, Sportplane Builder Publications, Austin, TX.

Brown, H.B. Jr and Zeglin, G. 1998. The bow leg hopping robot. *Proceedings of the IEEE International Conference on Robotics and Automation (ICRA)*, Leuven, Belgium, pp. 781–786.

DeMan, H., Lefeber, D., and Vermeulen, J. 1998. Design and control of a robot with one articulated leg for locomotion on irregular terrain. *Proceedings of the12th CISM-IFToMM Symposium on Theory and Practice of Robots and Manipulators*, Vienna, Austria, Springer-Verlag, Berlin, pp. 417–424.

Department of Defense. 2004. *Metallic Materials and Elements for Aerospace Vehicle Structures*, MIL-HDBK-5H.

Federal Aviation Administration. 2004. *Acceptable Methods, Techniques, and Practices—Aircraft Inspection and Repair*, AC43.13-1B.

Gambaryan, P.P. 1974. *How Mammals Run: Anatomical Adaptations*, Wiley, New York.

Heglund, N.C., and Taylor, C.R. 1988. Speed, stride frequency and energy cost per stride: how do they change with body size and gait? *Journal of Experimental Biology* 138:301–318.

Heglund, N.C., Taylor, C.R., and McMahon, T.A. 1974. Scaling of stride frequency and gait to animal size: mice to horses. *Science* 186:1112–1113.

Hildebrand, M. 1977. Analysis of asymmetrical gaits. *Journal of Mammalogy* 58(2):131–156.

Honeywell International, Inc. 2002. *Spectra Fiber 2000*. Available at http://www.spectrafiber.com/pdfs/hon-pf-ps10-sp2000.pdf.

Hoyt, D.F., and Taylor, C.R. 1981. Gait and the energetics of locomotion in horses. *Nature* 292:239–240.

Hutchinson, J.R., Famini, D., Lair, R., and Kram, R. 2003. Do fast-moving elephants run? *Nature* 422:493–494.

Jang, J.S.R., and Mizutani, E. 1996. Levenberg–Marquardt learning for ANFIS learning. Proceedings of the *1996 Biennial Conference of the North American Fuzzy Information Processing Society*, Berkeley, CA, pp. 87–91.

Jenkins, F.A. 1971. Limb posture and locomotion in the Virginia opossum (*Didelphis marsupialis*) and in other noncursorial mammals. *Journal of Zoology, London* 165:303–315.

Kimura, H., Akiyama, S., and Sakurama, K. 1999. Realization of dynamic walking and running of the quadruped using neural oscillator. *Autonomous Robots* 7:247–258.

Marhefka, D.W. 2000. *Fuzzy Control and Dynamic Simulation of a Quadruped Galloping Machine*, PhD Thesis, Ohio State University.

Marhefka, D.W., and Orin, D.E. 2000. Fuzzy control of quadrupedal running. *Proceedings of the IEEE International Conference on Robotics and Automation (ICRA)*, San Francisco, CA, pp. 3063–3069.

Marhefka, D.W., Orin, D.E., Schmiedeler, J.P., and Waldron, K.J. 2003. Intelligent control of quadruped gallops. *IEEE/ASME Transactions on Mechatronics* 8(4):446–456.

Mennitto, G., and Buehler, M. 1996. CARL: a compliant articulated robotic leg for dynamic locomotion. *Robotics and Autonomous Systems* 18:337–344.

Necsulescu, D., Sasiadek, J., Kim, B., and Green, D. 1993. Fusion of inertial and kinematic navigation systems for autonomous vehicles. *Proceedings of the IEEE–IEE Conference on Vehicle Navigation and Information Systems*, pp. 462–465.

Nichol, J.G., and Waldron, K.J. 2002. Biomimetic leg design for untethered quadruped gallop. *Proceedings of the 5th International Conference on Climbing and Walking Robots*, Paris, France, pp. 49–54.

Palmer, L., Orin, D., Marhefka, D., Schmiedeler, J., and Waldron, K. 2003. Intelligent control of an experimental articulated leg for a galloping machine. *Proceedings of the IEEE International Conference on Robotics and Automation (ICRA)*, Taipei, Taiwan, pp. 3821–3827.

Pandy, M.G., Kumar, V., Berme, N., and Waldron, K.J. 1988. The dynamics of quadrupedal locomotion. *ASME Journal of Biomechanical Engineering* 110:230–237.

Poulakakis, I., Smith, J.A., and Buehler, M. 2003. On the dynamics of bounding and extensions towards the half-bound and the gallop gaits. *Proceedings of the 2nd International Symposium of Adaptive Motion in Animals and Machines (AMAM)*, Japan.

Raibert, M.H. 1986. *Legged Robots that Balance*, MIT Press, Cambridge, MA.

Raibert, M.H. 1990. Trotting, pacing, and bounding by a quadruped robot. *Journal of Biomechanics* 23(1):79–98.

Raibert, M., Chepponis, M., and Brown, B. 1986. Running on four legs as though they were one. *IEEE Journal of Robotics and Automation* 2(2):270–282.

Renous, S., Gasc, J.-P., Bels, V.L., and Wicker, R. 2002. Asymmetrical gaits of juvenile *Crocodylus johnstoni*, galloping Australian crocodiles. *Journal of Zoology, London* 256:311–325.

Schmiedeler, J.P. 2001. *The Mechanics of and Robotic Design for Quadrupedal Galloping*. PhD dissertation, Department of Mechanical Engineering, Ohio State University.

Schmiedeler, J.P. and Waldron, K.J. 1999. The effect of drag on gait selection in dynamic quadrupedal locomotion. *International Journal of Robotics Research* 18(12):1224–1234.

Schmiedeler, J.P., and Waldron, K.J. 2000. Impact analysis as a design tool for the legs of mobile robots. *Advances in Robot Kinematics*, J. Lenarcic and M.M. Stanisic, editors, Kluwer Academic, Dortrecht, pp. 129–136.

Schmiedeler, J.P., and Waldron, K.J. 2002. Leg stiffness and articulated leg design for dynamic locomotion. *Proceedings of the ASME International Design Engineering Technical Conferences*, Montreal, Canada, Vol. 5B, pp. 1105–1112.

Waldron, K., Arkin, R., Bakkum, D., Merril, E., and Abdallah, M. 2003. Proprioceptive control for a robotic vehicle over geometric obstacles. *Proceedings of the IEEE International Conference on Robotics and Automation (ICRA)*, Taipei, Taiwan, pp. 109–114.